Three-dimensional superhydrophobic membranes via co-axial electrospinning for seawater desalination for membrane distillation

Journal of Materials Chemistry A

Yun Chul Woo[a,b,*], Minwei Yao[c], Wang-Geun Shim[d], Youngjin Kim[e], Leonard D. Tijing[c], Seung-Hyun Kim[f], and Ho Kyong Shon[c]

[a] Department of Land, Water and Environment Research, Korea Institute of Civil Engineering and Building Technology (KICT), 283, Goyang-Daero, Ilsanseo-Gu, Goyang-Si, Gyeonggi-Do, 10223, Republic of Korea

[b] Department of Construction and Environment Engineering, University of Science and Technology (UST), 217 Gajeong-Ro, Yuseong-Gu, Daejeon, 34113, Republic of Korea

[c] Centre for Technology in Water and Wastewater, School of Civil and Environmental Engineering, University of Technology Sydney (UTS). P. O. Box 123, 15 Broadway, NSW 2007, Australia

[d] Department of Polymer Science and Engineering, Sunchon National University, 255 Jungang-ro, Suncheon, Jeollanam-do, Republic of Korea

[e] Department of Environmental Engineering, Korea University, 2511, Sejong-ro, Jochiwon-eup, Sejong-si, 30019, Republic of Korea

[f] Department of Civil Engineering, Kyungnam University, Wolyoung-Dong, Changwon 631-701, Republic of Korea

Corresponding Author

*Y. C. Woo, E-mail: yunchul84@gmail.com, Tel: +82 31 910 0588, Fax: +82 31 910 0291

Abstract

Electrospun nanofiber membranes (ENMs) have some advantages such as high surface area, high hydrophobicity and porosity, and controllable pore size and membrane thickness. However, despite these advantages, ENMs still suffer from wetting issues in membrane distillation (MD). Co-axial electrospinning is a technique applied to fabricate suitable membranes for MD with improved wetting resistance. In the present study, we investigated poly(vinylidene fluoride-*co*-hexafluoropropylene) (PH) as the core and PH/silica aerogel (SiA) as the sheath to obtain superhydrophobic co-axial composite ENMs. The results of surface characterization indicated that the active layer (i.e., PH) of the co-axial ENMs was rough, highly porous (>80%), and superhydrophobic (contact angle >160º). Further, the co-axial ENMs possessed small pore sizes (<0.39 μm) and a suitable liquid entry pressure (>1.72 bar). Upon the application in long-term (one month) direct contact MD testing using a 3.5 wt% NaCl solution as the feed, a high water vapor flux and salt rejection of 14.5 L/m^{2}h and 99.99% were achieved, respectively, when applying the optimal 4 wt% SiA solution loading at the sheath. The ENMs fabricated using versatile co-axial electrospinning show great potential for long-term applications in direct contact MD desalination.

Keywords: Co-axial electrospinning, superhydrophobic, three-dimensional membrane, membrane distillation, electrospun nanofiber membrane (ENM)

1. Introduction

Membrane distillation (MD) is a non-isothermal membrane separation process applied in the treatment of saline or waste waters such as seawater, reverse osmosis brine, and textile and

dye wastewater.[1-4] The driving force of this process is the vapor pressure gradient between hot feed and cold permeate water. As a result, only water vapor can penetrate the hydrophobic porous membrane and condense at the permeate stream.[5, 6] MD is promising for portable and stand-alone desalination processes because it requires less pre-treatment than others. Moreover, it is possible to use non-corrosive and cheap plastic materials in compact MD systems due to the application of low hydraulic pressures in MD.[7] Nevertheless, owing to the lack of a suitably-designed MD membrane, a commercialized MD process has not yet been developed.[5] Although they were not specifically designed for application in MD processes, microfiltration membranes are commonly utilized, which results in severe wetting issues. Hence, the fabrication of suitable membranes in MD processes is required.[3]

Membrane properties including high porosity, adequate pore size and narrow pore size distribution, high hydrophobicity, and high liquid entry pressure (LEP) are required to improve the long-term stability and prevent wetting issues during MD operation.[8] Phase inversion is a commonly-used method to develop a membrane with suitable properties for MD process.[9] However, membranes fabricated by phase inversion generally do not have adequate porosity, pore size, and hydrophobicity for MD[3], resulting in lower membrane permeability. Recently, numbers of studies have introduced an electrospinning technique in the fabrication of MD membranes.[10, 11] Electrospinning is an alternative fabrication techniques for MD membranes[12] that offers a simple technique for the production of ultra-fine nanofiber membranes. A high electric field is applied to a polymer solution, resulting in the formation of elongated and stretched ultra-fine fibers that are collected on a rotating drum collector.[13] Electrospun nanofiber membranes (ENMs) have several advantages such as high surface area, high hydrophobicity and porosity, and controllable pore size and membrane thickness.[14, 15] In many studies, to some extent, the ENMs demonstrated improved MD performance; however, despite these improvements, the ENMs were still susceptible to wetting issues and had poor mechanical strength due to poor bonding between randomly oriented nanofibers.[16]

To overcome the wetting issues in MD, a three-dimensional hierarchical structure should be formed by the nanofibers in the membranes for higher surface roughness and hence better hydrophobicity. The three-dimensional hierarchical structure promotes the formation of air pockets on the membrane surface, which results in low surface contact between water droplets and the membrane surface. Hence, the adhesive forces between the membrane surface and water droplets are significantly reduced.[11, 17] As demonstrated in previous studies, the phenomenon of water roll-off from the membrane surface can be replicated, which leads to the self-cleaning behavior known as the "lotus effect".[17-19] Several recent studies reported the fabrication of "lotus effect" membranes using an electrospinning technique in conjunction with membrane modification as a post-treatment method, which had superhydrophobic membrane surfaces with a low sliding angle (SA) and a high water contact angle (CA).[17, 20-22] However, it was difficult to achieve membrane superhydrophobicity using these post-treatment methods, and the durability of the modified hydrophobic membrane surfaces against chemical cleaning was questionable.

The co-axial electrospinning technique is one of the most favorable and simple options to fabricate membranes with three-dimensional hierarchical structures.[18] Co-axial electrospinning is an enhanced electrospinning technique which produces fibers with core and sheath layers. The experimental set-up is composed of dual-tube nozzles, with one central tube immersed in the center of the annular tube, and two different polymer solutions, one for the core (central tube), and the other for the sheath (annular tube), which are separately injected into the co-axial nozzle with the subsequent simultaneously ejection producing dual-layer electrospun nanofibers.[18, 23] Using this simple technique, the morphology and characteristics from each polymer solution can be combined.[23] Three-dimensional hierarchical structure formation using co-axial electrospinning is a much more efficient method to achieve membrane surface superhydrophobicity compared with other modification methods such as layer-by-layer deposition, dip-coating, and the sol–gel method, and etc.[22, 24-26] Moreover, co-axial ENMs demonstrate higher thermal properties compared to those of conventional ENMs.[27] Therefore, co-axial electrospinning is a more attractive method to fabricate an ideal MD membrane.[16]

In the present study, we used poly(vinylidene fluoride-*co*-hexafluoropropylene) (PVDF-*co*-HFP, referred to herein as PH) as the core and PH/silica aerogel (SiA) as the sheath to produce a co-axial composite ENM and obtain a superhydrophobic membrane surface. The SiA was formed from silanol polar (Si-OH) groups with methyl ($-CH_3$) groups and methoxy ($-OCH_3$) groups, which are hydrophobic.[28] In addition, SiA exhibited a much lower thermal conductivity (≈0.02 W/mK) compared with that of conventional polymers such as polyvinylidene fluoride (0.22 W/mK), polypropylene (0.25 W/mK), and other nanoparticles such as carbon nanotubes and graphene, which led to increased water vapor flux during the MD process due to a reduction of conductive heat losses.[28-31] Furthermore, the incorporation of SiA into the sheath solution provides additional properties to the co-axial composite ENM, such as increased membrane roughness and hydrophobicity, which results in a highly efficient and sustainable MD membrane. The physical and chemical properties of the co-axial composite ENMs were examined and revealed improved membrane morphologies. The fabricated co-axial composite ENM exhibited superhydrophobicity, successfully repelling water from the membrane surface, which led to self-cleaning of the membrane surface. In addition, MD has mainly four different configurations, which are direct contact MD (DCMD), air gap MD (AGMD), vacuum MD (VMD) and sweeping gas MD (SGMD). Most studies conducted the DCMD process because of its simple configuration. However, DCMD has several disadvantages such as a low heat transfer resistance and high heat loss, which leads to a decrease in flux performance during long-term operations.[8] As a result, most of the studies using ENMs in DCMD applications operated for less than 50 hours although they exhibited a high water vapor flux performance.[10, 13, 14, 16, 32, 33] In the present study, we applied the DCMD process using the fabricated co-axial ENMs for 30 days (1 month). The flux and rejection performances of the as-spun neat PH and the co-axial composite ENMs were evaluated using 3.5 wt% sodium chloride (NaCl) as the feed solution. In order to realize the excellent properties of our co-axial composite ENM as an MD membrane, in this study we determine the optimal concentration of SiA in the sheath solution to fabricate a three-dimensional hierarchical co-axial composite ENM for sustainable operation in long-term MD processes.

2. Experimental methods

2.1. Materials

Poly(vinylidene fluoride-*co*-hexafluoropropylene) (PVDF-*co*-HFP, Mw = 450,000 g/mol, Kynar Powerflex® LBG) was purchased from Arkema Inc., and N,N-dimethylformamide (DMF), ethanol, and acetone were purchased from Sigma-Aldrich. Silica aerogel (JIOS AeroVa® powder, referred to herein as SiA) was purchased from JIOS. It has a pore diameter of less than 20 nm, particle size range of 1–20 μm, surface area of 600–1,000 m^2/g, and thermal conductivity of 0.016–0.021 W/mK. For the DCMD tests, sodium chloride (NaCl, Chem-supply) and deionized (DI) water were used. All chemicals were used as received.

2.2. Dope solutions for the core and sheath

The core solution of PH was prepared at a concentration of 18 wt% in 4:1 DMF/acetone under continuous stirring at room temperature for 1 d. For the sheath solution (referred to herein as PH-SiA), a given amount of SiA (2, 4 and 6 wt%) was first dispersed in a certain amount of DMF by bath sonication (Thermoline Scientific) for 3 h and then mixed with 7 wt% PH by magnetic stirring at room temperature for 1 d. **Table 1** shows the contents of the different core and sheath solutions and their respective codes used in this study.

[Table 1]

2.3. Co-axial electrospinning

Figure 1 shows a schematic diagram of the co-axial electrospinning set-up. The core and sheath solutions were each supplied in a 12 ml syringe attached to a single needle (17G-23G, inner diameter = 250 μm) and both needles were mounted on a co-axial adaptor. All the fabricated membranes were electrospun at an employed voltage, tip-to-collector distance, and core and sheath flow rates of 26 kV, 150 mm, 1.0 ml/h and 0.5 ml/h, respectively. Two syringe pumps

were used to maintain the required flow rate of the core and sheath solutions. All nanofibers were directly fabricated onto a rotating drum collector covered with aluminum foil. The co-axial adaptor was controlled by LabView software (National Instrument). The chamber humidity (30–40%) and temperature (18–23 °C) were maintained at constant values throughout the electrospinning process. After the completion of electrospinning, the membranes were peeled off the aluminum foil, transferred onto a baking paper and kept in a dry oven (OTWMHD24, LABEC) at 60 °C for 1 d to remove the residual solvents. The thickness of the fabricated ENMs was 140 ± 2 μm.

[Figure 1]

2.4. Direct contact membrane distillation

The DCMD set-up for performance test was the same as the one used in our previous work.[34] The fabricated and modified membranes were tested in a home-made DCMD set-up with an effective membrane area of 20 cm^2 and a channel dimension of 77 mm × 26 mm × 3 mm (L × W × H). The DCMD, using a counter-current flow set-up was carried out with constant inlet temperatures, which were 60.0 ± 1.5 °C and 20.0 ± 1.5 °C for the feed and coolant sides, respectively. The feed solution was a 3.5 wt% NaCl solution with total dissolved solids (TDS) of around 35 g/L and the permeate fluid was de-ionized (DI) water. The feed and permeate circulation rates were both maintained at 24 L/h. The inlet and outlet temperatures for both the feed and permeate streams were measured using a thermocouple. The concentration of the feed and permeate water was constantly measured with electrical TDS meters (HQ40d, Hach) throughout the tests.

2.5. Characterization and measurements

The surface and cross-sectional morphologies of the fabricated and modified electrospun membranes were observed using scanning electron microscopy (SEM, Zeiss Supra 55VP, Carl

Zeiss AG). Samples taken from each membrane were Au/Pd coated prior to SEM. The SEM images were carried out at an accelerating voltage of 10 kV, and multiple image magnifications at various areas were obtained for each sample.[8] In addition, the morphology of the neat PH and co-axial ENMs was observed using transmission electron microscopy (TEM, Tecnai T20, FEI Tecnai^{TM}). The membrane samples were placed on a 200 mesh copper grid (TED Pella Inc., CA, USA) and examined with high resolution TEM.[7]

The pore size of the co-axial ENMs was measured by capillary flow porometry (CFP-1200-AEXL). First, nitrogen (N_2) gas was applied to all the samples to determine the gas permeability, then the dry samples were wetted using Porefil (a wetting liquid with a low surface tension of 15.9 mN/m) and tested under the same conditions.[35]

The CA of the membranes was measured using the sessile drop method with an optical subsystem (Theta Lite 100) integrated with image-processing software. The membrane samples were placed on a flat platform and 5 µL droplets of water were applied to the surface. The water SA is a significant property for MD processes, and a small angle is expected for highly hydrophobic materials. The SA shows the difference between the advancing and receding CA, i.e., hysteresis.[36, 37] A 10 µL water droplet was placed on the membrane and the water droplet was gradually tilted until the water droplet started to slide on the membrane surface, and this tilting angle was recorded as the SA.[38]

LEP is a measurement of the ability of a hydrophobic membrane to resist pore wetting, and it was investigated using a homemade LEP set-up as shown in our previous work.[39] First, the reservoir was filled with 25 mL distilled water and then a dry membrane sample (effective surface area = 7 cm^2) was tightly secured in the cell. N_2 gas was then supplied and pressed through the bottom of the water-filled chamber, raising the pressure step wise and thereby pushing the water up to the membrane sample. The first appearance of bubbles on the top of the membrane was regarded as the LEP.

The membrane porosity, defined as the volume of pores divided by the total volume of the membrane, was measured via a gravimetric method.[39]

The membrane surface roughness was analyzed using atomic force microscopy (AFM) imaging. AFM was carried out under ambient conditions in non-contact mode with silicon probes (PUCOStation AFM, Surface Imaging Systems, Germany).[40]

A Fourier transform infrared spectroscope (FT-IR, Paragon 1000 spectrometer, PerkinElmer, USA) was used to gain the spectra of the membrane surface. All spectra were acquired by signal averaging 16 scans in the range of 500–4000 cm^{-1} at a resolution of 1 cm^{-1} in attenuated total reflection (ATR) mode.[7]

The thermal conductivity of the fabricated nanofiber membranes was measured using an LFA 447 Nanoflash® (NETZSCH, Australia). The analyzing machine worked according to ASTM E1461 at room temperature. The membranes were located on a furnace (Nanoflash 300), which was directly integrated into the sample changer of the LFA 447. The membrane analysis was carried out with a liquid nitrogen-cooled indium antimonide (InSb).

In order to confirm the textural properties of the neat PH and co-axial ENMs, nitrogen adsorption/desorption experiments were conducted at 77 K using a nanoPOROSITY adsorption analyzer (Mirae SI, Republic of Korea). The textural properties including specific surface area, pore volume, and pore size distributions were determined using the Brunauer–Emmett–Teller (BET), the Dubinin-Radushkevich (DR), and the Barrett-Joyner-Halenda (BJH) equations.[41-43] Additionally, the nitrogen adsorption energy distributions were calculated using the generalized nonlinear regularization method.[7]

3. Results and discussion

3.1. Morphologies and characteristics of the fabricated co-axial electrospun composite nanofiber membranes

Figure 2 shows the representative surface and cross-sectional SEM and TEM images of the fabricated neat and co-axial ENMs. In **Figure 2(a1–d1)**, it can be observed that the co-axial nanofibers have altered the morphology of the bead-on-string structures on the surface. Additionally, by increasing the SiA loading in the sheath solution, increasing amounts of beads

on the nanofiber surface were observed. The cross-sectional SEM images in **Figure 2(a2–d2)** appear to show a similar trend to the surface of the co-axial ENMs. Based on the SEM morphologies, the co-axial ENMs exhibited denser and a larger number of bead-on-string structures compared to the neat ENMs. Furthermore, characterization using TEM revealed the successfully fabricated nanofibers of the co-axial structure with the SiA particles on the nanofiber leading to increased surface roughness and higher hydrophobicity (**Fig. 2(a3–d3)**).

[Figure 2]

Figure 3 presents the fiber size distribution and pore size distribution of all the ENMs. The fiber size distribution of the ENMs (**Fig. 3(a1–d1)**) increased with an increasing concentration of the SiA dope solution, leading to a decreased fiber size distribution due to the different electric conductivities and solution viscosities of the doped solutions.[44] Similarly, the mean pore size of the ENMs also decreased (**Fig. 3(a2–d2)**). In MD processes, pore size and pore size distribution are significant factors in terms of preventing wetting issues and enhancing water vapor flux performance. To prevent wetting issues, the mean and maximum pore sizes of the electrospun MD membranes should be smaller than 0.6 μm, while to enhance the water vapor flux performance, the mean pore size of the MD membranes should be larger than 0.1 μm.[45] In **Figure 3** and **Table 2**, all of the co-axial electrospun membranes have mean pore sizes larger than 0.1 μm, which revealed that the co-axial electrospun membranes should demonstrate a high water vapor flux in MD processes. The maximum pore size of the co-axial ENMs was below 1.0 μm, which indicated that the co-axial ENMs may be wetted during MD processes.

In **Table 2**, the CA of the neat ENM revealed a highly hydrophobic properties, while the other co-axial ENMs exhibited a CA of over 150º. If a material and/or membrane has a CA over 150º, these materials have superhydrophobic property.[46, 47] Superhydrophobicity is one of the significant properties in MD processes, as it leads to increased anti-wetting resistance due to the

high surface roughness on the membrane surface. The co-axial ENMs, should, therefore, show improved operational stability compared to the neat ENMs.

Ultimately, the main factor that determines pore wetting is LEP rather than a high CA and maximum pore size.[44] All the co-axial ENMs showed an LEP of over 1.8 bar, which is similar to the ones of commercial PVDF membranes.[8] The co-axial ENMs can, therefore, prevent membrane pore wetting issues in MD processes albeit their larger maximum pore size.

[Figure 3]

[Table 2]

In **Table 2**, the SA for the neat ENM was not detected, which meant that the water droplet did not roll-off the neat ENM surface even though it was a highly hydrophobic material. This is called a petal surface effect. This is the surface property normally present in commercial flat-sheet membranes used in MD applications. In the present study, water droplets from the PH-SiA-2 co-axial ENMs started rolling off at an SA of 53.4°. The PH-SiA-4 and PH-SiA-6 co-axial ENMs revealed SAs of 3.2° and 2.8°, respectively, leading to an enhanced "lotus" surface effect compared to the PH-SiA-4 co-axial ENM.[48] This is attributed to the co-axial structure of the nanofiber membrane surface. Having lotus-like surface properties (or a three-dimensional structure on the membrane surface) facilitates self-cleaning, as the drops rolling of the surface carry some impurities away from the surface with them. Further, the lotus effect can also help to mitigate fouling and wetting problems during MD processes. Hence, this additional lotus effect property of the PH-SiA-4 and PH-SiA-6 co-axial ENMs has the potential to enhance the application of MD processes over a longer-term, as they possess improved anti-wetting properties and fouling resistance.

In order to produce large amounts of water permeation, high porosity and low thermal conductivity of the membrane are essential factors in MD. Most non-solvent induced phase

separation (NIPS) and thermally induced phase separation (TIPS) membranes have porosity below 80%, which is not enough in terms of water vapor flux for MD. In the present study, all the membranes exhibited over 85% porosity, indicating that the fabrication of a membrane with a porous structure is possible using the electrospinning technique. According to the results, an increased SiA concentration in co-axial electrospinning leads to a decreased porosity, due to solution properties, as mentioned above. Although the PH-SiA-6 co-axial ENM showed the lowest porosity, it may be sufficient for MD applications when compared to other membranes fabricated by NIPS and TIPS methods.

Among the other membrane properties, thermal conductivity is critical in relation to stability and flux performance during MD operation. If a membrane has a high thermal conductivity, it is not an adequate membrane as an increase in temperature polarization (TP) can occur, leading to decreased water vapor flux performance during MD operation.[49] The thermal conductivity of an MD membrane should be, therefore, as low as possible. As mentioned in the **Introduction**, the thermal conductivity of PVDF and PVDF-*co*-HFP polymeric membranes is between 0.20 $Wm^{-1}K^{-1}$ and 0.25 $Wm^{-1}K^{-1}$. Although these are low thermal conductivity values, lower values are required in order to decrease the thermal conductivity and allow long-term MD operation without decreasing flux performance.[31, 49] Due to the incorporation of SiA particles in the ENMs, the co-axial ENMs had thermal conductivity values approximately six times lower than the single nozzle ENM (**Table 2**). Based from the results, the co-axial ENMs should provide stable water vapor flux performance during MD processes, which will be conducted.

3.2. Hierarchical properties of the co-axial electrospun composite nanofiber membranes

The three-dimensional surface images of the fabricated ENMs are presented in **Figure 4**. The R_a, R_{ms}, and R_{max} values were measured using AFM imaging, and correspond to: mean roughness; root mean square of z values; and maximum vertical distance between the highest data points, respectively (**Table 3**).

In **Figure 4(a)**, it can be seen that the surface of the neat PH membrane was more flat compared to that of the other membranes (R_a of 284.65 ± 28.71 nm, R_{ms} of 358.71 ± 37.64 nm, and R_{max} of 1,841.52 ± 151.27 nm). Compared with the neat PH ENMs, the co-axial ENMs contained a large amount of particles, which were identified as SiA (**Fig. 4(b–d)**). The membrane surface roughness increased when the SiA concentration was increased, which led to increased hydrophobicity. It is expected that a membrane with a rough surface will have a high CA value.[39] Therefore, the high CA values of the co-axial ENMs can be explained by the increased surface roughness and the low surface tension of SiA. Thus, incorporation of SiA into the host polymer during membrane fabrication should result in an increased hydrophobicity of the membrane. **Table 2** shows that a high membrane CA leads to an increased membrane LEP, which can contribute to the prevention of wetting by the co-axial ENMs during the MD operation.

[Figure 4]

[Table 3]

3.3. Chemical properties of the co-axial electrospun composite nanofiber membranes

EDX measurement was carried out to further confirm the successful incorporation of SiA in/on the nanofiber (**Fig. 5(a)**). The atomic silica to fluorine (Si/F) ratio and silica to carbon (Si/C) showed increasing values with an increasing SiA content, which further confirms the successful dispersion and incorporation of SiA. **Figure 5(a)** indicates an increasing atomic silica concentration with an increasing amount of SiA incorporated in/on the membrane, suggesting the presence of increasing concentrations of SiA.

Figure 5(b) shows the FT-IR spectra of the fabricated ENMs. All of the neat and co-axial ENMs showed the same absorption bands attributed to the basic structural characteristics of PH at 837 cm^{-1}, 873 cm^{-1}, 1066 cm^{-1}, 1168 cm^{-1}, 1253 cm^{-1}, and 1404 cm^{-1}, which correspond to: CH_2 rocking and CF_2 asymmetric stretching (the β phase); CH_2 in-plane bending or rocking (the α

phase); C-C asymmetric stretching; C-C asymmetric stretching and CF_2 symmetric stretching; CF out-of-plane deformation (the β phase); and CF stretching vibrations or CH_2 wagging (the α phase), respectively.[50] Similar spectra were observed for the co-axial ENMs but at lower intensities, which signifies the presence of interfacial interactions (physical adsorption or weak chemical bonding) between PH and SiA particles. In addition, a new peak for the co-axial ENMs occurred at 750 cm^{-1}, which corresponds to Si-O symmetric stretching. Furthermore, the peak at 1066 cm^{-1} has increased intensity for the co-axial ENMs. The peak represented siloxane asymmetric bond stretching of Si-O-Si or Si-O-R groups (where R is a hydrocarbon such as $–CH_2CH_3$).

[Figure 5]

3.4. Textural properties of the co-axial electrospun composite nanofiber membranes

After incorporating the SiA nanoparticles into the PH solution, the observable porosity development was also noticed using nitrogen adsorption analysis. **Figure 6(a)** compares nitrogen adsorption and desorption isotherms of the neat ENM and the co-axial ENMs. All samples displayed type III or V isotherms with type H3 (or Type IIb) hysteresis loop in the relative pressure of 0.1-0.99 based on the IUPAC classification. The degree of hysteresis is slightly decreased after introducing the SiA into the PH (co-axial ENMs). This result supports the presence of slit shaped pores (or plate-like structures) in co-axial ENMs. In addition, the sharp increases were observed in the pressure range of 0.95-0.99, implying the existence of the large meso-macropores in the co-axial ENMs.

Figure 6(b) shows the pore size distributions determined using the BJH methods. The neat ENM represents bimodal distribution curve with two maxima: one at 2.4 nm and other at 54.4 nm. However unimodal distribution curves were obtained after introducing the SiA nanoparticles into the PH. In addition, as shown in **Figure 6(b)**, the portion of incremental pore volume moderately decreased at the large pore diameter range.

The textural properties of the neat ENM and the SiA incorporated PHs (co-axial ENMs) are also compared in **Table 4**. On the whole, the BET specific surface area and DR area of the ENMs are increased after adding the SiA into the PH except the PH-SiA-2. DR micropore volumes are slightly increased with the SiA content but BJH pore volumes were decreased with no consistent pattern. Such pattern can be partially explained by the substantial proportion of SiA nanoparticles, which can influence the pore networks of the neat ENM.

[Table 4]

[Figure 6]

Nitrogen adsorption energy distributions (AEDs) were calculated using general regularization method to further investigate the surface energetic heterogeneity characteristics. Here we used the Langmuir isotherm equation as a local isotherm. As compared in **Figure 7**, all samples represent two noticeable peaks indicating two distinct energy sites exist on the surface. It is interesting to note that the peak height and the peak width of the neat PH are higher and relatively narrower than those of SiA incorporated PHs (co-axial ENMs) in lower adsorption energy range (about 3-10 kJ/mol) but the reverse patterns were noticed in higher adsorption energy range (about 11-16 kJ/mol). These results clearly reveal that the co-axial ENMs have more energetic heterogeneous surface than those of the single-nozzle ENM.

[Figure 7]

3.5. Evaluations of DCMD performance test

The neat and co-axial ENMs fabricated in the present study were tested for their MD performance using the saline feed solution (3.5 wt% NaCl solution). Firstly, the flux and salt rejection performances of the neat and co-axial ENMs were evaluated and compared for a 72 h

test duration using the 3.5 wt% NaCl solution as the feed. After determining and comparing the individual performances of the membranes, the membrane with optimal performance was chosen and further evaluated in a long-term experiment, e.g. one month, to confirm the performance stability.

In **Figure 8**, the neat ENM exhibited higher average flux performance (11.07 L/m^{2}h (LMH)) compared to that of all the co-axial ENMs (5.87–10.57 LMH). The average flux performance of the PH-SiA-2 co-axial ENM was almost two times lower than that of the neat ENM, however the initial flux performance of the membrane was higher than that of the neat ENM. The water vapor flux performance of the neat ENM sharply increased after 48 h operation and the salt rejection of the membrane also decreased. Based on these results, it is worth to note that the neat ENM suffered a wetting problem during the DCMD operation due to its low LEP and CA, and large pore size and porosity. The neat ENM, therefore, was not a suitable membrane for seawater desalination using the DCMD process due to the wetting issue.

Figure 8(b) reveals the flux and salt rejection performance of the PH-SiA-2 co-axial ENM. The water vapor flux performance of the membrane drastically decreased between 0 h and 8 h, from 14.53 LMH to 4.73 LMH. The high water vapor permeability of the membrane led to an increased fouling rate due to depositions of NaCl crystals compared with that of a membrane with a low water vapor permeability.[16] Nevertheless, the salt rejection performance of the PH-SiA-2 co-axial ENM was maintained at 99.99%. The PH-SiA-2 co-axial ENM was, therefore, susceptible to fouling issues instead of membrane wetting issues.

However, the flux performance of the PH-SiA-4 and PH-SiA-6 co-axial ENMs did not decrease compared to that of the PH-SiA-2 co-axial ENM, which was the result of a higher SA. A high membrane SA can mitigate membrane fouling issues because foulants are not able to adhere to the membrane surface due to the self-cleaning property. As mentioned in **Sec 3.1.**, the PH-SiA-4 and PH-SiA-6 co-axial ENMs enhanced the long-term operation of the MD and did not suffer wetting and fouling problems due to the lower SA as a result of the lotus effect. In **Figure 8(c–d)**, the initial water vapor flux of the PH-SiA-4 and PH-SiA-6 ENMs was 13.30 LMH and

12.80 LMH, respectively. After 72 h, the final flux of both membranes was similar, with the initial flux of both membranes a result of low SAs and thermal conductivities.

Comparing with the PH-SiA-4 and PH-SiA-6 co-axial ENMs, the maximum pore size, mean pore size and porosity of the PH-SiA-4 co-axial ENM is slightly larger than those of the PH-SiA-6 co-axial ENM, leading to higher water vapor flux performance of the PH-SiA-4 co-axial ENM in the DCMD operation. Aside from obtaining a high flux performance, a stable and high salt rejection is also equally essential, if not more important, for MD applications, with a balance between these two properties being the most desirable. Based from the results, the PH-SiA-4 co-axial ENM showed optimal flux and salt rejection performances, which were consistent with the improvement in membrane characteristics and properties described in the previous sections. Therefore, PH-SiA-4 was selected for the long-term DCMD experiment.

[Figure 8]

3.6. Long-term experiment of DCMD by the co-axial electrospun composite nanofiber membrane

Figure 9(a) shows the water vapor flux and salt rejection performances of the PH-SiA-4 co-axial ENM over a long-term, one month, DCMD experiment. During the DCMD operation, the water vapor flux and salt rejection performances of the PH-SiA-4 co-axial ENM were maintained at 10.45 ± 0.63 LMH and 99.99%, respectively, which were similar to the 72 h DCMD results of the PH-SiA-4 co-axial ENM. Based on the results, the membrane operated well without wetting and fouling issues, due to its low SA and thermal conductivity properties. As mentioned in **Sec 3.1.**, TP is one of the significant drawbacks in MD. It can decrease water vapor flux performance during MD operation due to conductive heat losses. In particular, in terms of TP, DCMD is the worst configuration among the MD configurations due to the low heat transfer resistance and lower heat energy used for water evaporation.[51] Thus, it is more important to have a stable process than a high water vapor flux performance in DCMD operation. In the present

study, the water vapor flux performance of the PH-SiA-4 co-axial ENM was stable for the one month DCMD test. According to the results, the membrane is suitable for long-term MD applications as it possesses several important characteristics such as, low SA, low thermal conductivity, high LEP (thus avoiding TP), and reduced wetting and fouling problems whilst maintaining super-saturated high water vapor flux performance. A specific membrane may have a lower flux performance than other membranes, however if this membrane can prevent other drawbacks during MD operations, then this membrane is the most suitable option for MD.

In **Figure 9(b)**, the surface of the PH-SiA-4 co-axial ENM used in the long-term DCMD experiment was analyzed using SEM. The surface was similar to its virgin surface, without any deposits. Hence, the SEM results supports the observed stable flux and salt rejection performances for the one month DCMD operation. The stable flux performance and clear membrane surface of the PH-SiA-4 co-axial ENM could be attributed to the following reasons: 1) foulants were not able to adhere to the membrane due to the low SA of the surface (3.2^{o}), and 2) the low thermal conductivity of the membrane reduced conductive heat losses. 3) In general, the driving force of MD is the vapor pressure difference between the feed and permeate streams. Other membrane-based desalination technologies are pressure-driven separation processes, which have a higher fouling tendency compared to that of MD, therefore, the MD process has a lower fouling propensity process.

[Figure 9]

The behavior of the co-axial ENM and the single nozzle ENM are schematically presented in **Figure 10**. The simultaneous fabrication and modification achieved using co-axial electrospinning provides a three-dimensional structure on the surface of the co-axial nanofiber, leading to an increase in its surface roughness thus providing superhydrophobic properties and a surface lotus-effect, which result in increased anti-wetting and low thermal conductivity properties. Due to a decrease in conductive heat loss, and stable performance of the co-axial ENM

in the long-term DCMD is demonstrated.[31, 49] An SiA additive in the sheath solution is the key factor in providing low thermal conductivity and a three-dimensional structure, which drastically increases the long-term performance of the membranes in the long-term MD processes. We anticipated the SiA would fill the channels via the pores, due to the overlapping structure of the nanofiber, when the co-axial nanofiber was fabricated and modified, and that this would lead to a higher wetting resistance during the long-term MD operation. Such a SiA-containing membrane prevents leakage of salts due to its superhydrophobic properties and the surface lotus-effect, which can increase the LEP of the co-axial ENMs. This clearly shows the potential of the co-axial ENM for long-term MD processes for the treatment of seawater. Based from the results, it may be possible to apply the reported co-axial ENM in MD processes of longer durations than the one month presented in this study.

[Figure 10]

4. Conclusions

Poly(vinylidene fluoride-*co*-hexafluoropropylene) (PH) nanofiber membranes were successfully fabricated using a co-axial electrospinning technique. To confirm the increased wetting resistance, the simultaneously fabricated and modified ENMs were evaluated in a long-term DCMD process for one month using 3.5 wt% NaCl as the feed. The results suggest that the simple and simultaneous fabrication and modification of the ENMs using co-axial electrospinning without complicated multiple stage to fabricate and modify membranes, provided increased hydrophobic properties via the formation of a three-dimensional structure on the membrane surface. This led to improved wetting resistance properties of the co-axial ENMs, due to an increased loading of SiA providing increased surface roughness and therefore superhydrophobic properties. The optimal concentration of SiA was found to be 4 wt% (the PH-SiA-4 ENM), which resulted in a high CA and low SA, in turn leading to a high wetting resistance and high LEP (1.91 bar). These improved properties along with the low thermal conductivity of SiA translate to high flux (initial flux of 14.53 L/m^{2}h) and salt rejection (99.99%) performances for the PH-SiA-4

ENMs. The stability of the membranes was demonstrated by the excellent water vapor flux and salt rejection performances of the membranes over a long-term, one month, DCMD operation. It is worth to note that it is more important to have a stable process than a high water vapor flux performance in a commercially available MD process. The results signify that the co-axial ENMs have strong potential for the treatment of seawater solutions without suffering from wetting issues, and may be the appropriate membrane for pilot-scale and real-scale MD applications.

Acknowledgments

This research was supported by a grant (code-NRF-2017M1A2A2047369) from research program funded by National Research Foundation of Korea (NRF), Republic of Korea. This study was also funded by the Korea Ministry of Environment (MOE) and Korea Environmental Industry & Technology Institute (KEITI) as "Industrial Facilities & Infrastructure Research Program [146667].

References

1. S. Lin, N. Y. Yip and M. Elimelech, *Journal of Membrane Science*, 2014, **453**, 498-515.
2. A. K. An, J. Guo, S. Jeong, E. J. Lee, S. A. Tabatabai and T. Leiknes, *Water Res*, 2016, **103**, 362-371.
3. S. Nejati, C. Boo, C. O. Osuji and M. Elimelech, *Journal of Membrane Science*, 2015, **492**, 355-363.
4. X. Wu, Q. Jiang, D. Ghim, S. Singamaneni and Y.-S. Jun, *Journal of Materials Chemistry A*, 2018, **6**, 18799-18807.
5. Z. Wang, D. Hou and S. Lin, *Environ Sci Technol*, 2016, **50**, 3866-3874.
6. J. Zuo, S. Bonyadi and T.-S. Chung, *Journal of Membrane Science*, 2016, **497**, 239-247.
7. Y. C. Woo, L. D. Tijing, W.-G. Shim, J.-S. Choi, S.-H. Kim, T. He, E. Drioli and H. K. Shon, *Journal of Membrane Science*, 2016, **520**, 99-110.

8. Y. C. Woo, L. D. Tijing, M. J. Park, M. Yao, J.-S. Choi, S. Lee, S.-H. Kim, K.-J. An and H. K. Shon, *Desalination*, 2017, **403**, 187-198.

9. H. Maab, L. Francis, A. Al-saadi, C. Aubry, N. Ghaffour, G. Amy and S. P. Nunes, *Journal of Membrane Science*, 2012, **423-424**, 11-19.

10. Y. Liao, R. Wang, M. Tian, C. Qiu and A. G. Fane, *Journal of Membrane Science*, 2013, **425-426**, 30-39.

11. Y. Liao, C. H. Loh, R. Wang and A. G. Fane, *ACS Appl Mater Interfaces*, 2014, **6**, 16035-16048.

12. J. H. Kim, S. H. Park, M. J. Lee, S. M. Lee, W. H. Lee, K. H. Lee, N. R. Kang, H. J. Jo, J. F. Kim, E. Drioli and Y. M. Lee, *Energy Environ. Sci.*, 2016, **9**, 878-884.

13. L. D. Tijing, Y. C. Woo, M. A. H. Johir, J.-S. Choi and H. K. Shon, *Chemical Engineering Journal*, 2014, **256**, 155-159.

14. Y. Liao, R. Wang and A. G. Fane, *Journal of Membrane Science*, 2013, **440**, 77-87.

15. E.-J. Lee, A. K. An, T. He, Y. C. Woo and H. K. Shon, *Journal of Membrane Science*, 2016, DOI: 10.1016/j.memsci.2016.07.019.

16. B. S. Lalia, E. Guillen-Burrieza, H. A. Arafat and R. Hashaikeh, *Journal of Membrane Science*, 2013, **428**, 104-115.

17. Y. Liao, R. Wang and A. G. Fane, *Environ Sci Technol*, 2014, **48**, 6335-6341.

18. N. Nuraje, W. S. Khan, Y. Lei, M. Ceylan and R. Asmatulu, *J. Mater. Chem. A*, 2013, **1**, 1929-1946.

19. J. Lee, C. Boo, W. H. Ryu, A. D. Taylor and M. Elimelech, *ACS Appl Mater Interfaces*, 2016, **8**, 11154-11161.

20. C. Boo, J. Lee and M. Elimelech, *Environ Sci Technol*, 2016, **50**, 8112-8119.

21. S. Lin, S. Nejati, C. Boo, Y. Hu, C. O. Osuji and M. Elimelech, *Environmental Science & Technology Letters*, 2014, **1**, 443-447.

22. Y. C. Woo, Y. Chen, L. D. Tijing, S. Phuntsho, T. He, J.-S. Choi, S.-H. Kim and H. K. Shon, *Journal of Membrane Science*, 2017, **529**, 234-242.

23. D. Han and A. J. Steckl, *Langmuir*, 2009, **25**, 9454-9462.

24. J. Meng, C. H. Lau, Y. Xue, R. Zhang, B. Cao and P. Li, *Journal of Materials Chemistry A*, 2020, **8**, 8462-8468.

25. Y. C. Woo, Y. Kim, M. Yao, L. D. Tijing, J. S. Choi, S. Lee, S. H. Kim and H. K. Shon, *Environ Sci Technol*, 2018, **52**, 2186-2196.

26. C.-Y. Huang, C.-C. Ko, L.-H. Chen, C.-T. Huang, K.-L. Tung and Y.-C. Liao, *Separation and Purification Technology*, 2016, DOI: 10.1016/j.seppur.2016.12.037.

27. Z. Zhang, G. Sui, H. Bi and X. Yang, *Journal of Membrane Science*, 2015, **492**, 77-87.

28. A. Soleimani Dorcheh and M. H. Abbasi, *Journal of Materials Processing Technology*, 2008, **199**, 10-26.

29. Z. Li, Y. Peng, Y. Dong, H. Fan, P. Chen, L. Qiu and Q. Jiang, *Applied Surface Science*, 2014, **317**, 338-349.

30. J. Wu, K. R. Zodrow, P. B. Szemraj and Q. Li, *Journal of Materials Chemistry A*, 2017, **5**, 23712-23719.

31. J. Pan, C. Xiao, Q. Huang, H. Liu and J. Hu, *Journal of Materials Chemistry A*, 2015, **3**, 23549-23559.

32. J. A. Prince, G. Singh, D. Rana, T. Matsuura, V. Anbharasi and T. S. Shanmugasundaram, *Journal of Membrane Science*, 2012, **397-398**, 80-86.

33. M. Yao, Y. C. Woo, L. D. Tijing, W.-G. Shim, J.-S. Choi, S.-H. Kim and H. K. Shon, *Desalination*, 2016, **378**, 80-91.

34. L. D. Tijing, Y. C. Woo, W.-G. Shim, T. He, J.-S. Choi, S.-H. Kim and H. K. Shon, *Journal of Membrane Science*, 2016, **502**, 158-170.

35. M. Tian, Y. Yin, C. Yang, B. Zhao, J. Song, J. Liu, X.-M. Li and T. He, *Desalination*, 2015, **369**, 105-114.

36. M. Jin, X. Feng, J. Xi, J. Zhai, K. Cho, L. Feng and L. Jiang, *Macromolecular Rapid Communications*, 2005, **26**, 1805-1809.

37. G. R. J. Artus, S. Jung, J. Zimmermann, H. P. Gautschi, K. Marquardt and S. Seeger, *Advanced Materials*, 2006, **18**, 2758-2762.

38. P. v. d. Valk, A. W. J. v. Pelt, H. J. Busscher, H. P. d. Jong, C. R. H. Wildevuur and J. Arends, *Journal of Biomedical Materials Research*, 1983, **17**, 807-817.

39. Y. C. Woo, Y. Kim, W.-G. Shim, L. D. Tijing, M. Yao, L. D. Nghiem, J.-S. Choi, S.-H. Kim and H. K. Shon, *Journal of Membrane Science*, 2016, **513**, 74-84.

40. Y. Kim, S. Lee, J. Kuk and S. Hong, *Desalination*, 2015, **367**, 154-160.

41. S. Brunauer, P. H. Emmett and E. Teller, *Journal of the American Chemical Society*, 1938, **60**, 309-319.

42. M. M. Dubinin, *Carbon*, 1985, **23**, 373-380.

43. E. P. Barrett, L. G. Joyner and P. P. Halenda, *Journal of the American Chemical Society*, 1951, **73**, 373-380.

44. L. D. Tijing, J.-S. Choi, S. Lee, S.-H. Kim and H. K. Shon, *Journal of Membrane Science*, 2014, **453**, 435-462.

45. D. Lee, Y. C. Woo, K. H. Park, S. Phuntsho, L. D. Tijing, M. Yao, W.-G. Shim and H. K. Shon, *Journal of Membrane Science*, 2020, **598**.

46. H. Zhou and Z. Guo, *Journal of Materials Chemistry A*, 2019, **7**, 12921-12950.

47. X. An, G. Xu, B. Xie and Y. Hu, *Journal of Materials Chemistry A*, 2019, **7**, 2376-2384.

48. L. Deng, P. Li, K. Liu, X. Wang and B. S. Hsiao, *Journal of Materials Chemistry A*, 2019, **7**, 11282-11297.

49. S. Cao, X. Wu, Y. Zhu, R. Gupta, A. Tan, Z. Wang, Y.-S. Jun and S. Singamaneni, *Journal of Materials Chemistry A*, 2020, **8**, 5147-5156.

50. Y. C. Woo, J. J. Lee, L. D. Tijing, H. K. Shon, M. Yao and H.-S. Kim, *Desalination*, 2015, **369**, 51-61.

51. B. B. Ashoor, S. Mansour, A. Giwa, V. Dufour and S. W. Hasan, *Desalination*, 2016, **398**, 222-246.

Table list:

Table 1 Dope solutions for core and sheath used for co-axial electrospinning in the present study

Membrane code	The core solution			The sheath solution		
	PH[a] (wt%)	DMF[b] (wt%)	Acetone (wt%)	PH[a] (wt%)	DMF[b] (wt%)	SiA[c] (wt%)
Neat PH	18	65.6	16.4	-	-	-
PH-SiA-2	18	65.6	16.4	7	91	2
PH-SiA-4	18	65.6	16.4	7	89	4
PH-SiA-6	18	65.6	16.4	7	87	6

[a] Polyvinylidene fluoride-*co*-hexafluoropropylene

[b] N, N-dimethylformamide

[c] Silica aerogel

Table 2 Characteristics of the membranes used in the present study

Membrane code	Thickness (μm)	Mean pore	Maximum	Porosity (%)	LEP (bar)	CA[a] (deg)	SA[b] (deg)	Thermal conductiv

		size (μm)	pore size (μm)					ity ($Wm^{-1}K^{-1}$)
Neat PH	141.8 ± 1.2	0.58	1.03	93.2 ± 1.3	1.45 ± 0.11	143.8 ± 2.5	N.D[c]	0.207 ± 0.026
PH-SiA-2	139.7 ± 2.1	0.38	0.93	90.6 ± 2.2	1.87 ± 0.14	151.5 ± 3.5	53.4 ± 2.2	0.033 ± 0.000
PH-SiA-4	140.5 ± 1.7	0.39	0.97	89.7 ± 1.6	1.91 ± 0.15	166.2 ± 0.5	3.2 ± 0.2	0.031 ± 0.000
PH-SiA-6	141.3 ± 1.8	0.36	0.95	87.3 ± 2.5	1.97 ± 0.13	169.7 ± 0.7	2.8 ± 0.2	0.033 ± 0.000

[a] CA = Contact angle

[b] SA = Sliding angle

[c] N.D = Not detected

Table 3 AFM analyses of the neat PH and co-axial electrospun nanofiber membranes

	Neat PH	PH-SiA-2	PH-SiA-4	PH-SiA-6
R_a (nm)	284.65 ± 28.71	331.05 ± 56.02	451.15 ± 161.83	488.43 ± 221.39
R_{ms} (nm)	358.71 ± 37.64	427.80 ± 76.60	632.39 ± 201.60	633.97 ± 282.05

R_{max} (nm)	1,841.52 ± 151.27	3,266.26 ± 772.78	4,050.94 ± 455.73	5,339.75 ± 2436.16

Table 4 Textural properties of the neat PH, PH-SiA-2, PH-SiA-4 and PH-SiA-6 membranes

		Neat PH	PH-SiA-2	PH-SiA-4	PH-SiA-6
Surface Area, m^2/g	BET	61	54	99	113
	DR	14	22	21	56
Pore volume, cc/g	BJH	0.98	0.48	0.65	0.37
	DR	0.006	0.010	0.011	0.024

Figure list:

Figure 1 Schematic diagram of (A) the co-axial electrospinning ((a) syringe pumps, (b) core solution, (c) sheath solution, (d) co-axial adaptor, (e) co-axial nanofiber, (f) rotating drum collector, (g) metal plate, and (h) high voltage power supply) and (B) single-nozzle electrospinning ((a) syringe pump, (b) polymer solution, (c) single-nozzle adaptor, (d) single nanofiber, (e) rotating drum collector, (f) metal plate, and (g) high voltage power supply).

Figure 2 (a1, b1, c1, d1) Surface and (a2, b2, c2, d2) cross-sectional SEM images and (a3, b3, c3, d3) TEM images of (a1, a2, a3) the neat PH, (b1, b2, b3) PH-SiA-2, (c1, c2, c3) PH-SiA-4 and (d1, d2, d3) PH-SiA-6 membranes.

Figure 3 (a1, b1, c1, d1) Fiber size distribution and (a2, b2, c2, d2) pore size distribution of (a1, a2) the neat PH, (b1, b2) PH-SiA-2, (c1, c2) PH-SiA-4 and (d1, d2) PH-SiA-6 membranes. Average fiber size of the neat PH, PH-SiA-2, PH-SiA-4 and PH-SiA-6 was 234.94 μm, 115.82 μm, 86.18 μm and 68.27 μm, respectively. Mean pore size of the neat PH, PH-SiA-2, PH-SiA-4 and PH-SiA-6 was 0.58 μm, 0.38 μm, 0.39 μm and 0.36 μm, respectively.

Figure 4 AFM images of (a) the neat PH, (b) PH-SiA-2, (c) PH-SiA-4 and (d) PH-SiA-6 membranes. The mean roughness (Ra) of the neat PH, PH-SiA-2, PH-SiA-4 and PH-SiA-6 membranes was 284.65 ± 28.71 nm, 331.05 ± 156.60 nm, 451.15 ± 161.83 nm and 488.43 ± 221.39 nm, respectively.

Figure 5 (a) C/Si and F/Si ratio by EDX and (b) ATR-FTIR peaks of the neat PH, PH-SiA-2, PH-SiA-4 and PH-SiA-6 membranes.

Figure 6 (a) Nitrogen adsorption and desorption isotherms and (b) BJH pore size distributions obtained from the desorption isotherm for the neat PH, PH-SiA-2, PH-SiA-4 and PH-SiA-6 membranes.

Figure 7 Comparison of nitrogen adsorption energy distributions calculated for the neat PH, PH-SiA-2, PH-SiA-4 and PH-SiA-6 membranes.

Figure 8 (a – d) Flux and salt rejection performances of (a) the neat PH, (b) PH-SiA-2, (c) PH-SiA-4 and (d) PH-SiA-6 membranes for 72 h operation in DCMD process. Feed water was 3.5 wt% NaCl solution (TDS = 35 g/L). Feed and permeate flow rates were both maintained at 24 L/h. Feed and permeate temperatures were 60 ± 1.5 ºC and 20 ± 1.5 ºC, respectively. Average water vapor flux of the neat PH, PH-SiA-2, PH-SiA-4 and PH-SiA-6 was 11.07 LMH, 5.87 LMH, 10.57 LMH and 9.40 LMH, respectively. Initial water vapor flux of the neat PH, PH-SiA-2, PH-SiA-4 and PH-SiA-6 was 8.98 LMH, 14.53 LMH, 13.30 LMH and 12.80 LMH, respectively.

Figure 9 (a) Flux and salt rejection performances of the PH-SiA-4 co-axial electrospun nanofiber membrane in DCMD application for 1 month (31 d). Feed water was 3.5 wt% NaCl solution (TDS = 35 g/L). Feed and permeate flow rates were both maintained at 24 L/h. Feed and permeate flow rates were both maintained at 24 L/h. Feed and permeate temperatures were 60 ± 1.5 °C and 20 ± 1.5 °C, respectively. Average water vapor flux of the PH-SiA-4 co-axial electrospun nanofiber membrane for 31 d was 10.45 ± 0.63 LMH. (b) Surface SEM image of the PH-SiA-4 co-axial electrospun nanofiber membrane after 1 month DCMD test.

Figure 10 Schematic illustrations of the co-axial electrospun nanofiber membrane fabricated by co-axial electrospinning and the neat PH electrospun nanofiber membrane fabricated by single-nozzle electrospinning used in the present study and their properties.

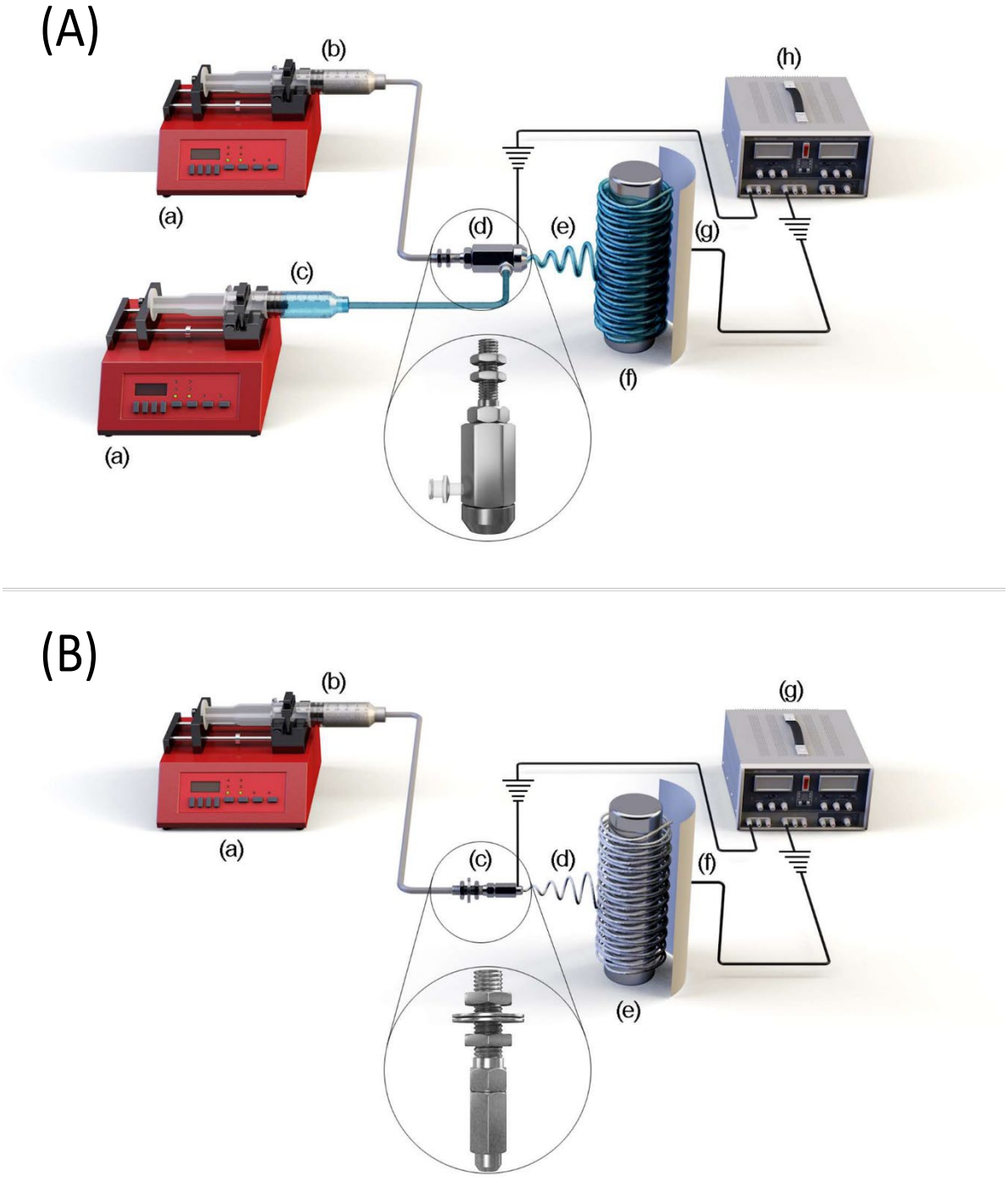

Figure 1 Schematic diagram of (A) the co-axial electrospinning ((a) syringe pumps, (b) core solution, (c) sheath solution, (d) co-axial adaptor, (e) co-axial nanofiber, (f) rotating drum collector, (g) metal plate, and (h) high voltage power supply) and (B) single-nozzle electrospinning ((a) syringe pump, (b) polymer solution, (c) single-nozzle adaptor, (d) single nanofiber, (e) rotating drum collector, (f) metal plate, and (g) high voltage power supply).

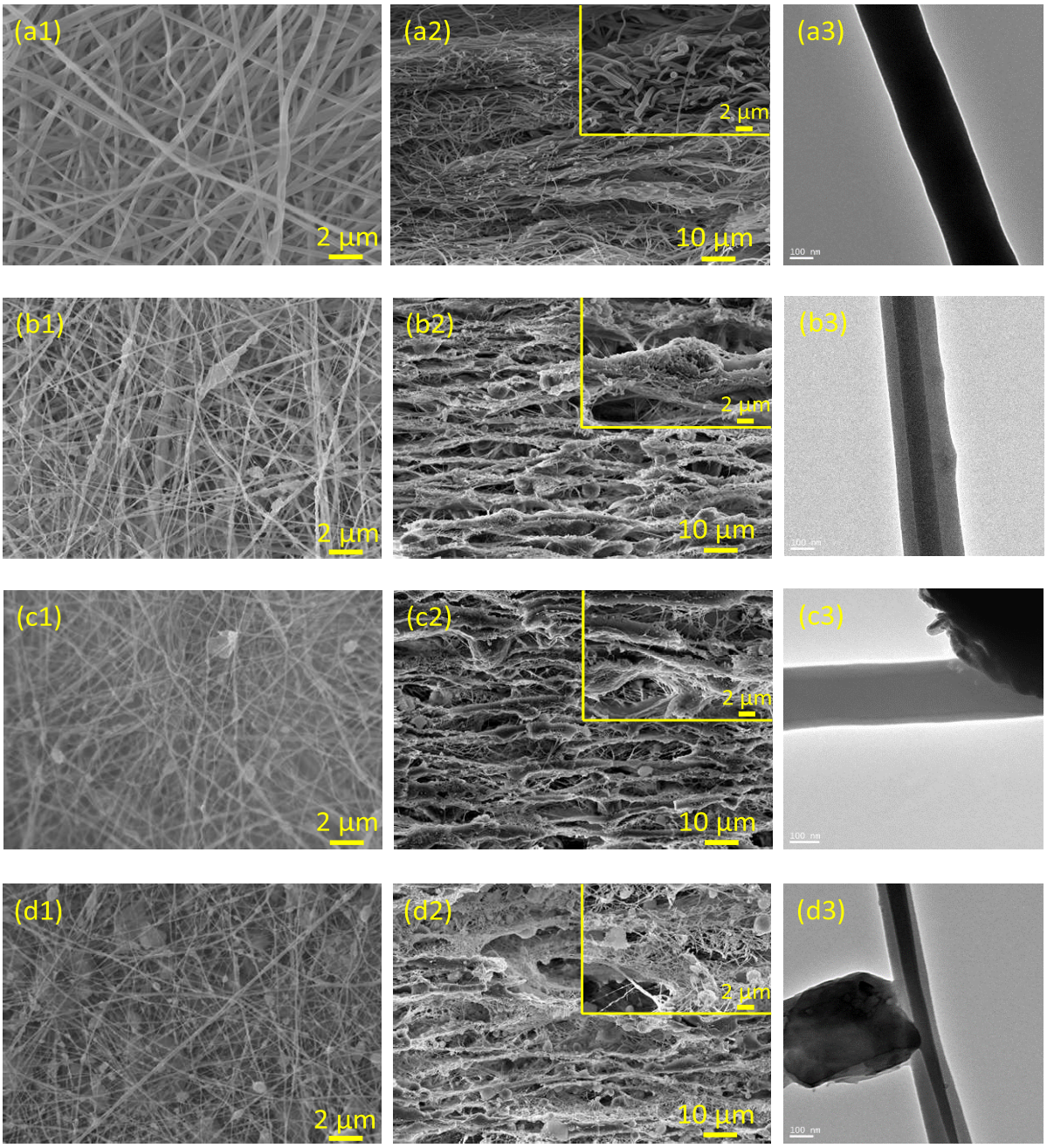

Figure 2 (a1, b1, c1, d1) Surface and (a2, b2, c2, d2) cross-sectional SEM images and (a3, b3, c3, d3) TEM images of (a1, a2, a3) the neat PH, (b1, b2, b3) PH-SiA-2, (c1, c2, c3) PH-SiA-4 and (d1, d2, d3) PH-SiA-6 membranes.

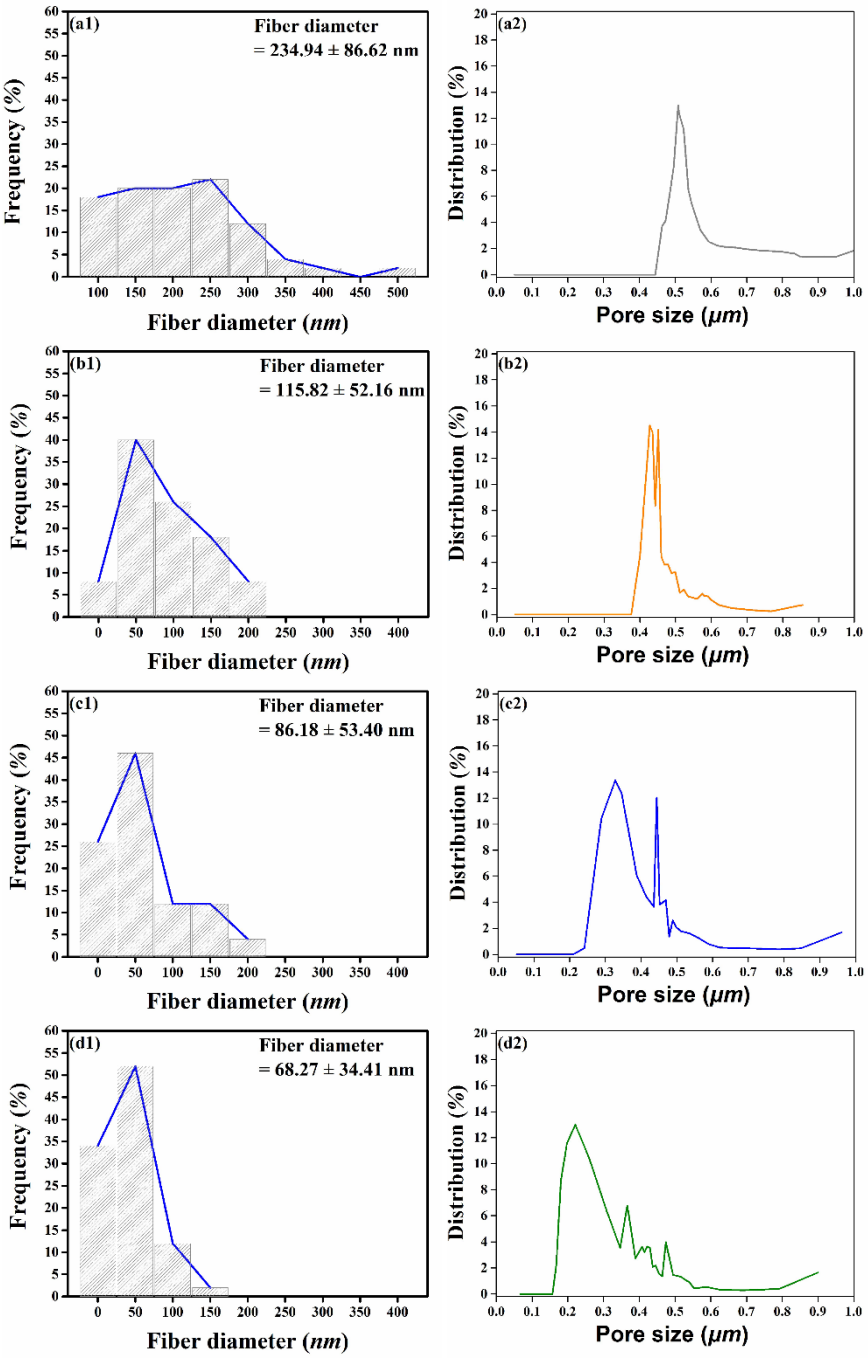

Figure 3 (a1, b1, c1, d1) Fiber size distribution and (a2, b2, c2, d2) pore size distribution of (a1, a2) the neat PH, (b1, b2) PH-SiA-2, (c1, c2) PH-SiA-4 and (d1, d2) PH-SiA-6 membranes. Average fiber size of the neat PH, PH-SiA-2, PH-SiA-4 and PH-SiA-6 was 234.94 μm, 115.82 μm, 86.18 μm and 68.27 μm, respectively. Mean pore size of the neat PH, PH-SiA-2, PH-SiA-4 and PH-SiA-6 was 0.58 μm, 0.38 μm, 0.39 μm and 0.36 μm, respectively.

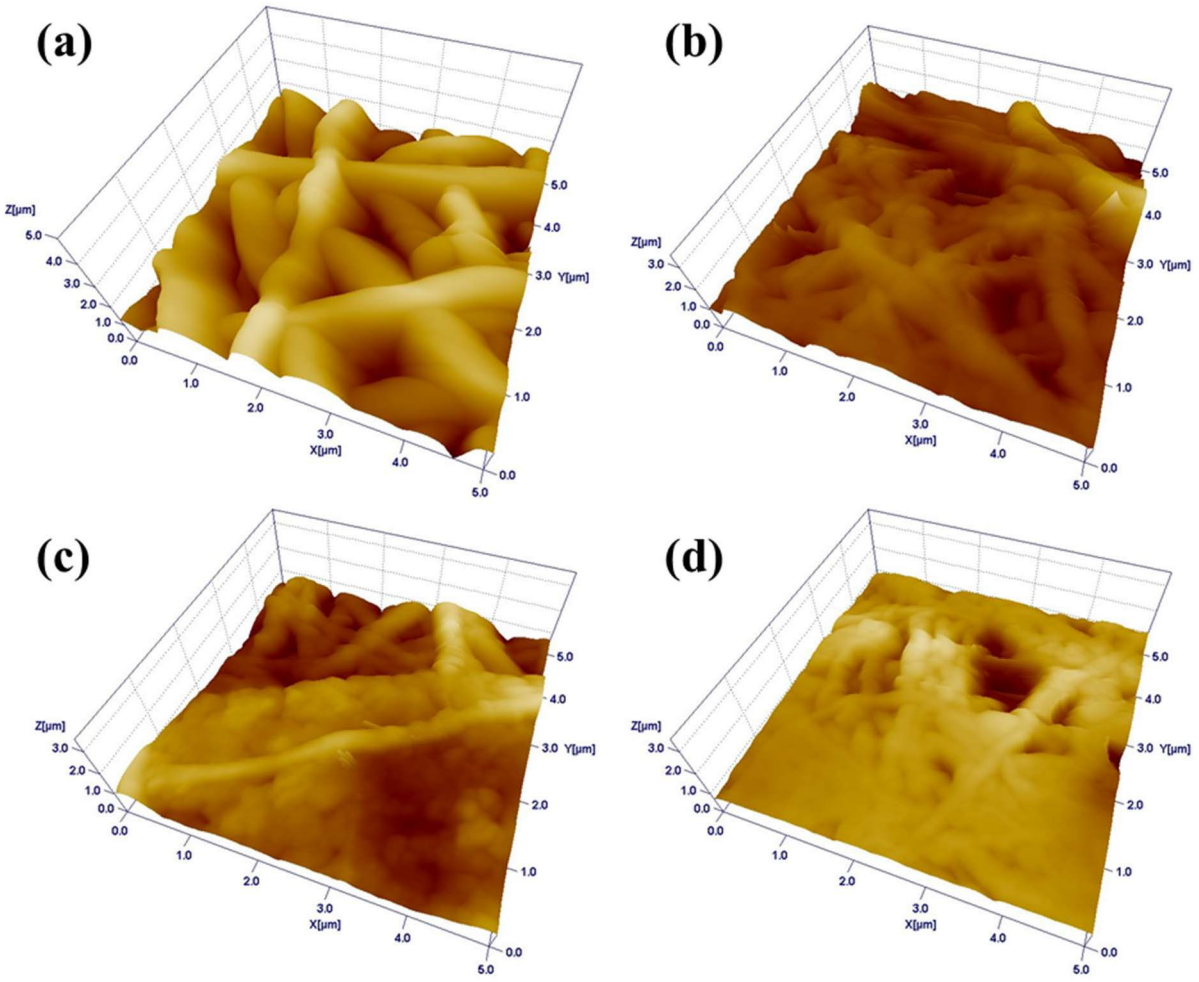

Figure 4 AFM images of (a) the neat PH, (b) PH-SiA-2, (c) PH-SiA-4 and (d) PH-SiA-6 membranes. The mean roughness (Ra) of the neat PH, PH-SiA-2, PH-SiA-4 and PH-SiA-6 membranes was 284.65 ± 28.71 nm, 331.05 ± 156.60 nm, 451.15 ± 161.83 nm and 488.43 ± 221.39 nm, respectively.

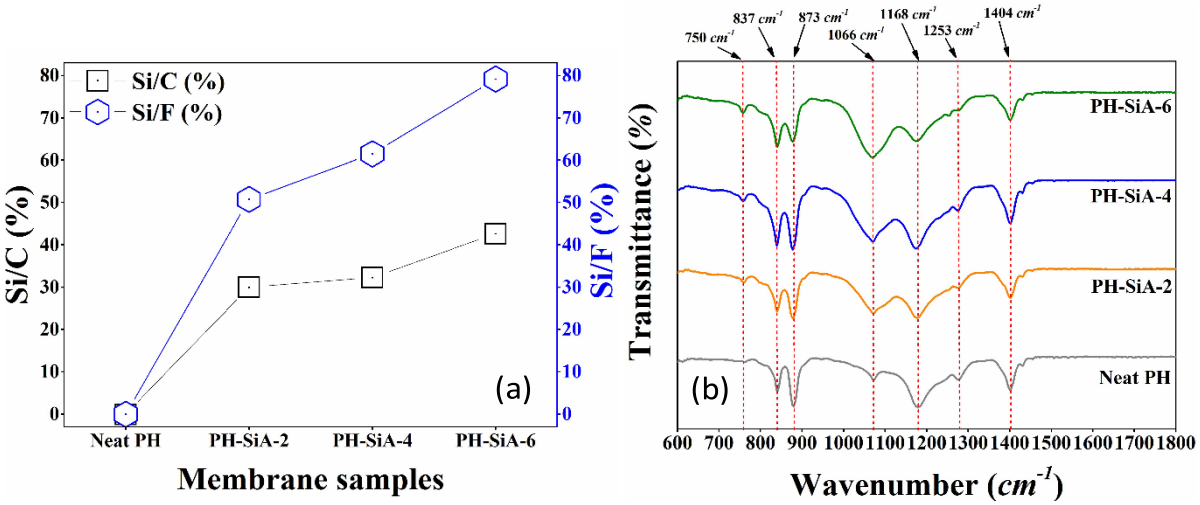

Figure 5 (a) C/Si and F/Si ratio by EDX and (b) ATR-FTIR peaks of the neat PH, PH-SiA-2, PH-SiA-4 and PH-SiA-6 membranes.

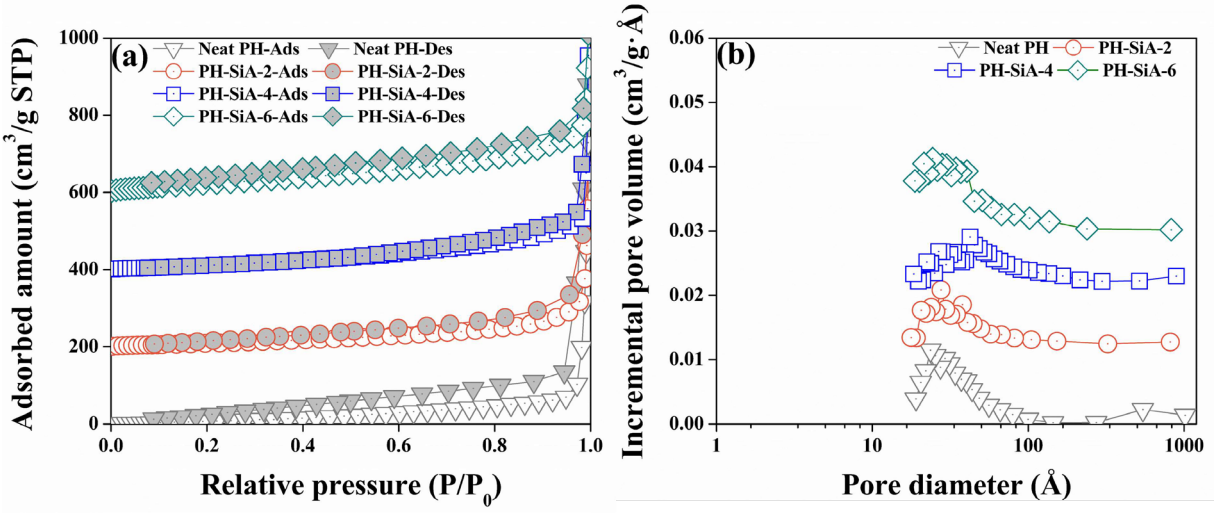

Figure 6 (a) Nitrogen adsorption and desorption isotherms and (b) BJH pore size distributions obtained from the desorption isotherm for the neat PH, PH-SiA-2, PH-SiA-4 and PH-SiA-6 membranes.

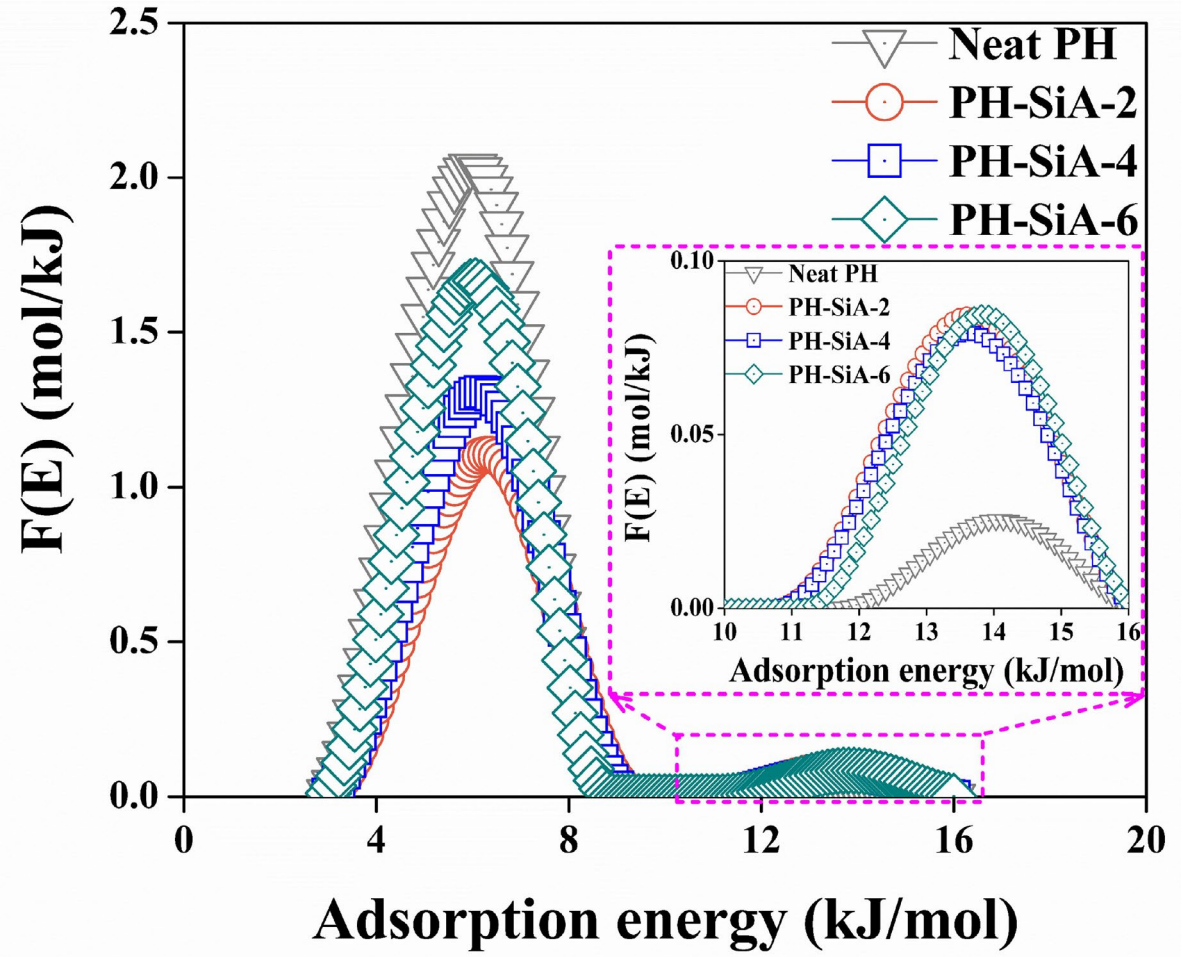

Figure 7 Comparison of nitrogen adsorption energy distributions calculated for the neat PH, PH-SiA-2, PH-SiA-4 and PH-SiA-6membranes.

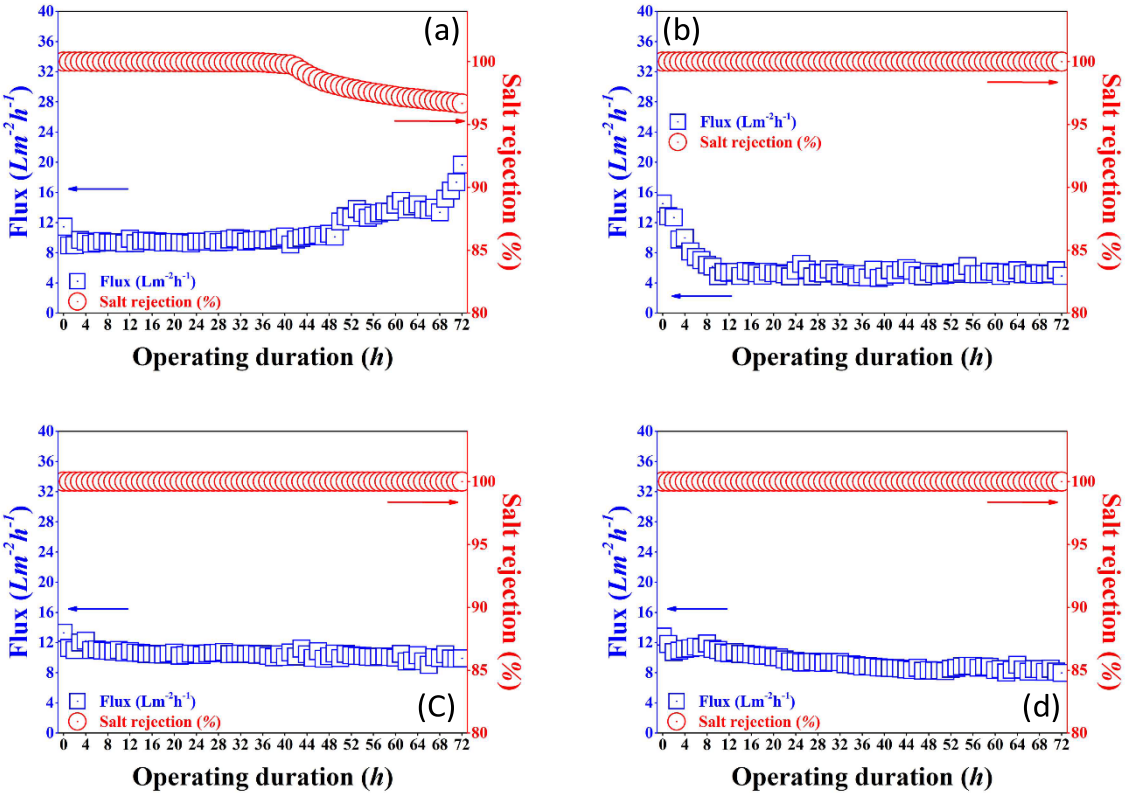

Figure 8 (a – d) Flux and salt rejection performances of (a) the neat PH, (b) PH-SiA-2, (c) PH-SiA-4 and (d) PH-SiA-6 membranes for 72 h operation in DCMD process. Feed water was 3.5 wt% NaCl solution (TDS = 35 g/L). Feed and permeate flow rates were both maintained at 24 L/h. Feed and permeate temperatures were 60 ± 1.5 ºC and 20 ± 1.5 ºC, respectively. Average water vapor flux of the neat PH, PH-SiA-2, PH-SiA-4 and PH-SiA-6 was 11.07 LMH, 5.87 LMH, 10.57 LMH and 9.40 LMH, respectively. Initial water vapor flux of the neat PH, PH-SiA-2, PH-SiA-4 and PH-SiA-6 was 8.98 LMH, 14.53 LMH, 13.30 LMH and 12.80 LMH, respectively.

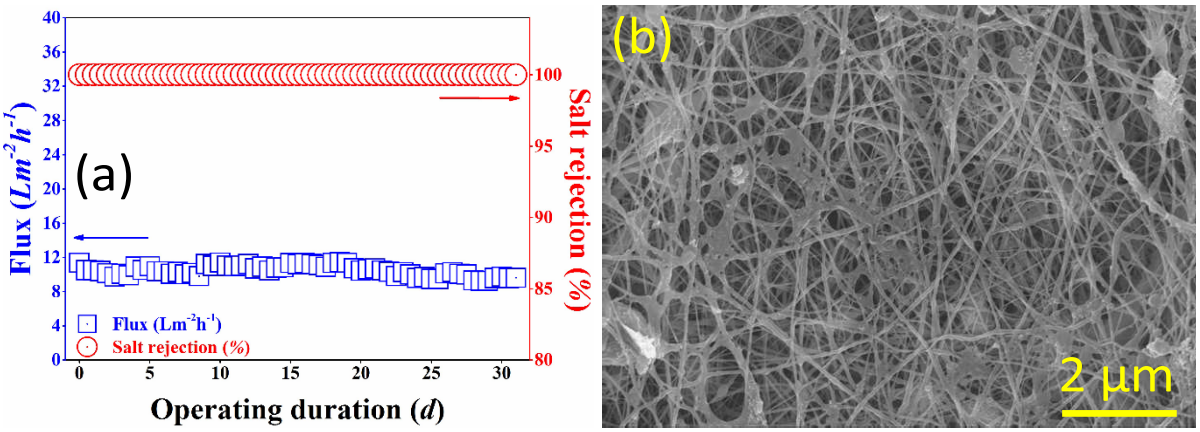

Figure 9 (a) Flux and salt rejection performances of the PH-SiA-4 co-axial electrospun nanofiber membrane in DCMD application for 1 month (31 d). Feed water was 3.5 wt% NaCl solution (TDS = 35 g/L). Feed and permeate flow rates were both maintained at 24 L/h. Feed and permeate flow rates were both maintained at 24 L/h. Feed and permeate temperatures were 60 ± 1.5 °C and 20 ± 1.5 °C, respectively. Average water vapor flux of the PH-SiA-4 co-axial electrospun nanofiber membrane for 31 d was 10.45 ± 0.63 LMH. (b) Surface SEM image of the PH-SiA-4 co-axial electrospun nanofiber membrane after 1 month DCMD test.

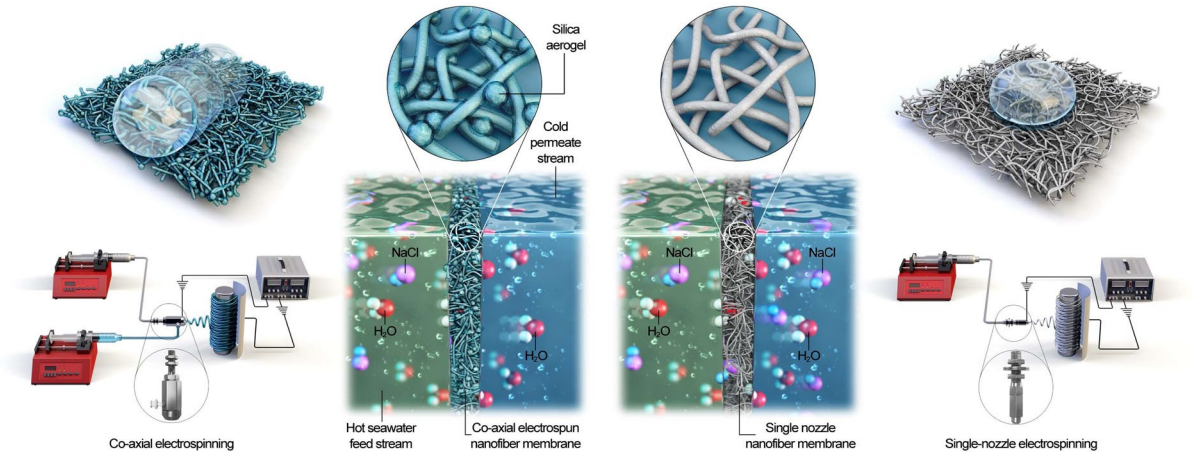

Figure 10 Schematic illustrations of the co-axial electrospun nanofiber membrane fabricated by co-axial electrospinning and the neat PH electrospun nanofiber membrane fabricated by single-nozzle electrospinning used in the present study and their properties.